Computer Assisted Mechanics and Engineering Sciences, 6: 385–402, 1999.

Two-dimensional dynamic simulation of fracture and fragmentation of solids

Ferenc Kun[1,3*], Gian Antonio D'Addetta[2], Hans J. Herrmann[1] and Ekkehard Ramm[2]

[1] *Institute for Computer Applications (ICA1), University of Stuttgart, Pfaffenwaldring 27, D-70569 Stuttgart, Germany*

[2] *Institute for Structural Mechanics, University of Stuttgart, Pfaffenwaldring 7, D-70550 Stuttgart, Germany*

[3] *Department of Theoretical Physics, Kossuth Lajos University, P.O.Box 5, H-4010 Debrecen, Hungary*

(Received March 8, 1999)

We present a two-dimensional discrete model of solids that allows us to follow the behavior of the solid body and of the fragments well beyond the formation of simple cracks. The model, consisting of polygonal cells connected via beams, is an extension of discrete models used to study granular flows. This modeling is particularly suited for the simulation of fracture and fragmentation processes. After calculating the macroscopic elastic moduli from the cell and beam parameters, we present a detailed study of an uniaxial compression test of a rectangular block, and of the dynamic fragmentation processes of solids in various experimental situations. The model proved to be successful in reproducing the experimentally observed subtleties of fragmenting solids.

1. Introduction

Fracture and fragmentation of solids are difficult problems to handle numerically due to the creation and continuous motion of new surfaces. Commonly used numerical methods solve partial differential equations of continuum mechanics. With classical numerical methods such as Finite Elements (FE), Finite Differences (FD) or Boundary Elements (BE) a small number of discontinuities may be considered but these methods cannot encompass the entire fracturing process.

The alternative approach is the Discrete Element Method (DEM) in which the elastic medium is considered to be fully discontinuous, i.e. the elastic solid is assembled of discrete elements. The microscopic interaction of the elements is defined such that the model accounts for the macroscopic elastic behavior of materials. The time evolution of the model is followed by solving numerically the equation of motion of the individual elements (Molecular Dynamics (MD)). This model construction results in a "simulated solid" and the modeling of a specific process of a material is referred to as simulation. The inter-element contacts can be considered as grain boundaries which define the possible paths for crack propagation. Hence, in these models it is easy to take into account spatial inhomogeneities. Historically this method of treatment of solids was initiated by the discrete model of Cundall [3, 4] which was proposed to study the behavior of granular materials. Following his ideas several discrete models of solids have been introduced recently by "gluing" together discrete elements symbolizing grains of the material [14, 15, 17].

In this paper we present a two-dimensional model for a deformable, breakable, granular solid by connecting unbreakable, undeformable elements by elastic beams. The contacts between the particles can be broken according to a physical breaking rule, which takes into account the stretching and

* Corresponding author

bending of the connections. The breaking rule contains two parameters to describe the relative importance of the two breaking modes. The main goal of the paper is to demonstrate the abilities of our model in the study of material's destruction. After measuring the macroscopic elastic behavior of the material, widespread applications of the model will be presented, i.e. the model will be applied to study the fracture of a rectangular solid block in compression, and the catastrophic fragmentation of solids due to impact and explosion.

2. The model

Our model of a deformable, breakable granular solid is an extension of those models which are used to study the behavior of granular materials applying randomly shaped convex polygons to symbolize grains [18]. The construction of the model is composed of three major steps. Namely, the implementation of the granular structure of the solid, the determination of the interaction of grains, and finally capturing the breaking of the solid. This section gives a detailed overview of the three steps of the model construction.

2.1. Granularity

In order to take into account the complex structure of the granular solid we use arbitrarily shaped convex polygons, i.e. we divide the solid into grains by a Voronoi cellular structure. The Voronoi construction is a random tessellation of the plane into convex polygons. In general, this is obtained by putting a random set of points onto the plane and then assigning each point that part of the plane which is nearer to it than to any other point. In our case, to get an initial configuration of the polygons we construct a so-called vectorizable random lattice, which is a Voronoi construction with slightly reduced disorder (see [10]). It is performed by first putting a regular grid onto the plane and throwing points randomly and independently in each square of the grid with a maximal distance a from the center of the squares. Using these points for the Voronoi construction, the randomness of the tessellation can be controlled by tuning the value of the parameter a between 0

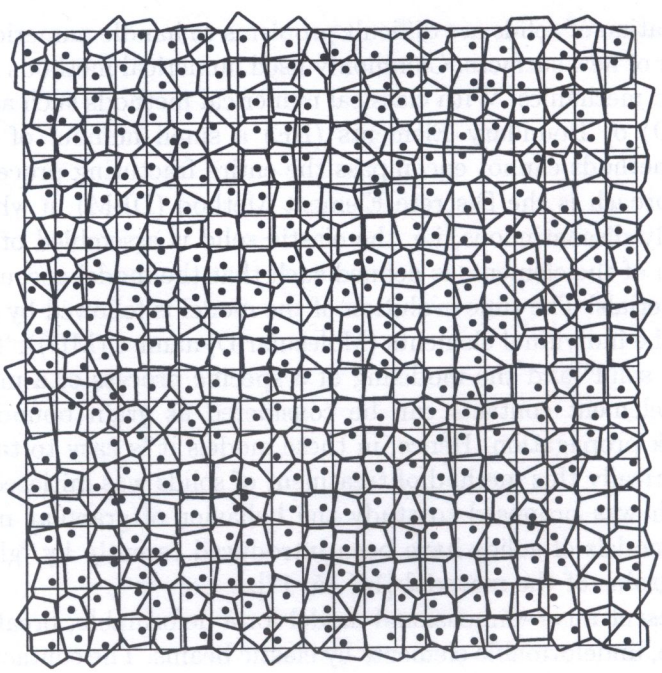

Fig. 1. Construction of the vectorizable random lattice. The dots indicate the points used for the tessellation. These points were thrown independently and randomly onto the squares of the regular grid

and the lattice spacing of the grid. Figure 1 presents an example of the vectorizable random lattice including the underlying grid, the random points used for the tessellation and the final polygonal structure. The advantage of the vectorizable random lattice compared to the ordinary Poissonian Voronoi tessellation is that the number of neighbors of each polygon is limited which makes the computer code faster and allows us to simulate larger systems.

The convex polygons of this Voronoi construction are supposed to model the grains of the material, see also [18]. This way the structure of the solid is built on a mesoscopic scale. Each element is thought of as a large collection of atoms, however, in the simulation these polygons are the smallest particles interacting elastically with each other. The polygons have three continuous degrees of freedom in two dimensions: the two coordinates of the center of mass and the rotation angle.

2.2. Elastic behavior of the solid

In the framework of the discrete element approach the elastic behavior of the solid is captured by defining proper interactions on the mesoscopic level, between the polygons. In the case of spherical particles the Hertz contact law provides the force between two particles as a function of the overlap distance. For randomly shaped particles it is impossible to derive such a simple interaction law, hence, we introduce an approximate method.

The polygons are considered to be rigid bodies. They are not breakable and not deformable but they can overlap when they are pressed against each other. The overlap represents up to some extent the local deformation of the grains. Usually the overlapping polygons have two intersection points which define the contact line (see Fig. 2). The total force $\vec{F}_{ij}$ acting between polygons i and j can be decomposed into normal F_{ij}^N and tangential F_{ij}^T components with respect to the contact line, i.e.

$$\vec{F}_{ij} = F_{ij}^N \cdot \vec{n} + F_{ij}^T \cdot \vec{t}, \tag{1}$$

where $\vec{n}$ denotes the unit vector pointing in the direction perpendicular to the contact line, and $\vec{t}$ is the tangential unit vector.

In order to simulate the elastic contact force between touching grains we introduce a repulsive force between the overlapping polygons. This force is proportional to the overlapping area A divided by a characteristic length L_c of the interacting polygon pair. Our choice of L_c is given by

$$\frac{1}{L_c} = \frac{1}{2}\left(\frac{1}{r_i} + \frac{1}{r_j}\right),$$

where r_i, r_j are the diameters of circles of the same area as the polygons. This normalization is necessary in order to reflect the fact that the spring constant is proportional to the elastic modulus divided by a characteristic length. (In the case of a linear spring this characteristic length is simply

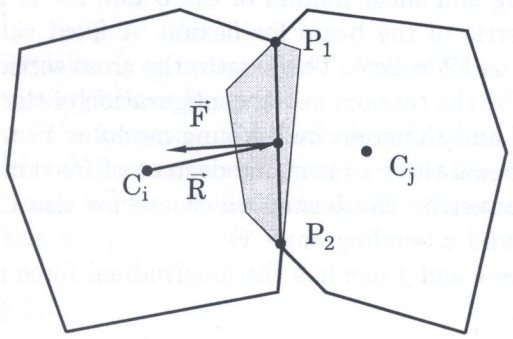

Fig. 2. To calculate the elastic contact force $\vec{F}$ between two particles one has to obtain the overlap area. The intersection points P_1, P_2 define the contact line $P_1\vec{P}_2$. The force is applied at the center of the contact line $\vec{R}$ and the direction of the force is perpendicular to $P_1\vec{P}_2$

the equilibrium length of the spring.) The direction of the force is chosen to be perpendicular to the contact line of the polygons. The contact force $\vec{F}_{ij}$ between two particles is given by

$$\vec{F}_{ij} = -\frac{YA}{L_c}\vec{n}, \tag{2}$$

where Y is the grain bulk Young modulus, see also Fig. 2. Damping and the friction of the touching polygons according to Coulomb's friction law can also be implemented. The complete form of the normal force F_{ij}^N contains the contribution of the elastic force and the damping, while the tangential component F_{ij}^T is responsible for the friction:

$$F_{ij}^N = -\frac{YA}{L_c} - m_{ij}^{\text{eff}} \cdot \gamma_N \cdot v_{\text{rel}}^N, \tag{3}$$

$$F_{ij}^T = \min(-m_{ij}^{\text{eff}}\gamma_T |v_{rel}^T|, \mu |F_{ij}^N|), \tag{4}$$

$$\vec{v}^{rel} = \vec{v}_j - \vec{v}_i, \tag{5}$$

$$m_{ij}^{\text{eff}} = \frac{m_i \cdot m_j}{m_i + m_j}, \tag{6}$$

where m_i denotes the mass of polygon i, γ_N is the damping coefficient, γ_T and μ are the friction coefficients.

In order to keep the solid together it is necessary to introduce a cohesion force between neighboring polygons. For this purpose we introduce beams, which were extensively used recently in crack growth models [7, 6]. The centers of mass of neighboring polygons are connected by elastic beams, which exert an attractive, restoring force between the grains, and can break in order to model the fragmentation of the solid. Because of the randomness contained in the Voronoi-tessellation the lattice of beams is also random. An example of a random lattice of beams coupled to the Voronoi polygons can be seen in Fig. 3.

A beam between sites i and j is thought of as having a certain cross section S^{ij} giving to it not only longitudinal but also shear elasticity. This cross section is the length of the common side of the neighboring polygons in the initial configuration. The length of the beam l^{ij} is defined by the distance of the centers of mass. The elastic behavior of the beams is governed by two material dependent constants. For the beam between sites i and j:

$$a^{ij} = \frac{l^{ij}}{ES^{ij}}, \tag{7}$$

$$b^{ij} = \frac{l^{ij}}{GS^{ij}}, \tag{8}$$

$$c^{ij} = \frac{l^{ij^3}}{EI^{ij}}, \tag{9}$$

where E and G are the Young and shear moduli of the beam, S^{ij} is the area of the beam section, and I^{ij} is the moment of inertia of the beam for flexion. A fixed value of E was used for all the beams and b^{ij} was chosen to be $b^{ij} = 2a^{ij}$. The length, the cross section and the moment of inertia of each beam are determined by the random initial configuration of the polygons as explained above. The beam Young modulus E and the grain bulk Young modulus Y are, in principal, independent.

In the local frame of the beam three continuous degrees of freedom are assigned to both lattice sites (centers of mass) connected by the beam, which are for site i, the two components of the displacement vector (u_x^i, u_y^i) and a bending angle Θ^i.

For the beam between sites i and j one has the longitudinal force acting at site i:

$$F_x^i = \alpha^{ij}(u_x^j - u_x^i), \tag{10}$$

the shear force

$$F_y^i = \beta^{ij}(u_y^j - u_y^i) - \frac{\beta^{ij} l^{ij}}{2}(\Theta^i + \Theta^j), \tag{11}$$

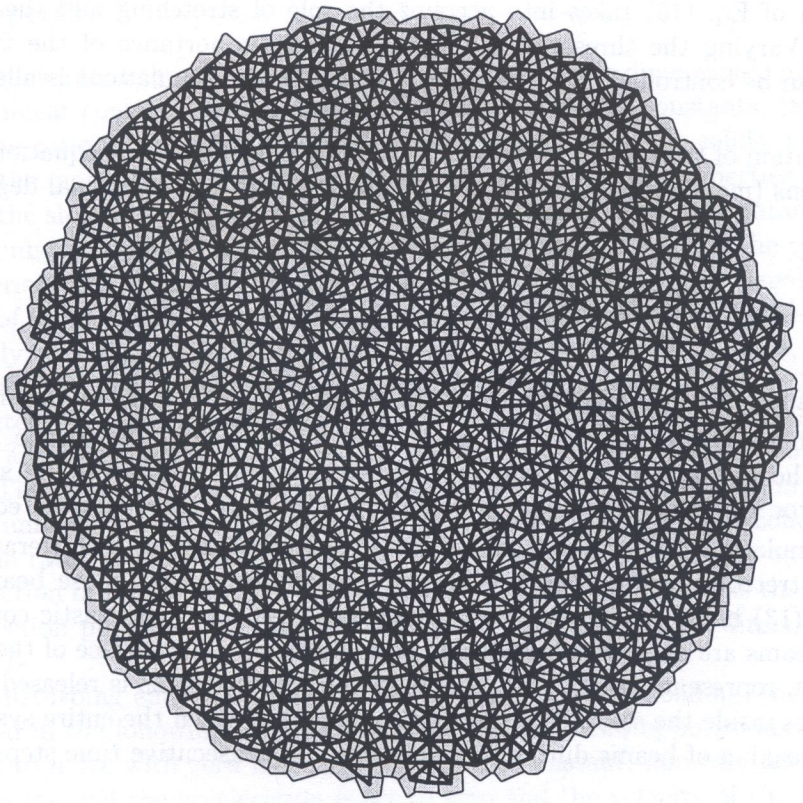

Fig. 3. Elastic beams connecting the Voronoi polygons in a disc-shaped sample. Due to the randomness in the Voronoi tessellation the lattice of beams is also random

and the flexural torque at site i

$$M_z^i = \frac{\beta^{ij} l^{ij}}{2}(u_y^j - u_y^i + l^{ij}\Theta^j) + \delta^{ij} l^{ij^2}(\Theta^j - \Theta^i), \tag{12}$$

where

$$\alpha^{ij} = \frac{1}{a^{ij}}, \qquad \beta^{ij} = \frac{1}{b^{ij} + \frac{1}{12}c^{ij}}, \quad \text{and} \quad \delta^{ij} = \beta^{ij}\left(\frac{b^{ij}}{c^{ij}} + \frac{1}{3}\right).$$

It can be shown that this beam model is a discretisation of the simplified Cosserat — equations of continuum elasticity which should be used to describe the elastic behavior of the granular solids, instead of the Lamé equations [16].

2.3. Breaking of the solid

To model fracture and fragmentation it is necessary to complete the model with a breaking rule, according to which the over-stressed beams break.

For not too fast deformations the breaking of a beam is only caused by stretching and bending. We impose a breaking rule which takes into account these two breaking modes, and which can reflect the fact that the longer and thinner beams are easier to break. We used a breaking rule of the form of the von Mises plasticity criterion [7]:

$$\left(\frac{\epsilon}{t_\epsilon}\right)^2 + \frac{\max(|\Theta^1|, |\Theta^2|)}{t_\Theta} \geq 1, \tag{13}$$

where $\epsilon = \Delta l / l$ is the longitudinal strain of the beam, Θ^1 and Θ^2 are the rotation angles at the two ends of the beam and t_ϵ and t_Θ are threshold values for the two breaking modes. In the simulations we used the same threshold values t_ϵ and t_Θ for all the beams.

The first term of Eq. (13) takes into account the role of stretching and the second term the role of bending. Varying the threshold values the relative importance of the two modes in the beam breaking can be controlled. The breaking of beams in the simulations is allowed solely under stretching.

The time evolution of the system is followed by solving numerically the equation of motion of the individual polygons (molecular dynamics) for the translational and rotational degrees of freedom:

$$m_i \ddot{\vec{r}}_i = \sum_{j=1}^{N} \vec{F}_{ij}\,, \qquad I_i^p \ddot{\Theta}_i = \sum_{j=1}^{N} M_z^{ij}, \qquad i = 1, \ldots, N, \tag{14}$$

where N is the total number of polygons in the sample, and I_i^p denotes the moment of inertia of polygon i with respect to its center of mass. The force $\vec{F}_{ij}$ and the torque M_z^{ij} contains the contribution of the polygon-polygon contacts and that of the beams. In the simulation code a Predictor-Corrector scheme of fifth order is used for the solution of the Newton equations Eq. (14).

During the simulation the left hand side of Eq. (13) is evaluated at each iteration time step for all the existing stretched beams. The breaking of beams means that those beams for which the condition of Eq. (13) holds are removed from the calculation, i.e. their elastic constants are set to zero. Removed beams are never restored during the simulation. The surface of the grains, on which beams are broken, represents cracks. The energy of the broken beams is released in creating these new crack surfaces inside the solid. The simulation is stopped when the entire system gets relaxed, i.e. there is no breaking of beams during some hundreds of consecutive time steps.

3. Applications

To demonstrate the capabilities and to test the limitations of our model we have performed a variety of simulations, which fall into three categories: (1) measuring the macroscopic elastic moduli of the model solid, (2) strain controlled compressive strength test, and (3) catastrophic fragmentation of solids due to explosion and impact. Since fracture in compression, and fragmentation in impact and in explosion occurs very rapidly most of the available experimental results were obtained from the analysis of the debris in the final, relaxed state of the processes. Hence, in several cases there is no possibility for direct quantitative comparison of the simulation results to the experimental ones. In these cases only qualitative comparison could be performed. The parameter values used in the simulations are summarized in Table 1.

Table 1. The parameter values used in the simulations

Parameter	*Symbol*	*Unit*	*Value*
Density	ρ	g/cm^3	5
Grain bulk Young modulus	Y	dyn/cm^2	10^{10}
Beam Young modulus	E	dyn/cm^2	$5 \cdot 10^9$
Time step	dt	s	10^{-6}
Diameter of the disc	d	cm	40
Average # of polygons	n		1100
Energy of the explosion	E_o	erg	$5 \cdot 10^9$
Average initial speed	v_o	m/s	200
Estimated sound speed	c	m/s	900

3.1. Elastic properties

In [14, 15] it was shown that the macroscopic elastic behavior of two dimensional materials composed of particles with linear contacts can be characterized by two elastic constants, the Young modulus K and the Poisson ratio ν, similar to the case of homogeneous isotropic solids. It seems clear from the definition of the model that these elastic constants depend on the properties of the constituent particles, i.e. on the shape of the grains, on the stiffness of the grain–grain contacts (in our context the grain bulk Young modulus Y and the beam Young modulus E) and on the typical grain size.

For real materials the Young modulus K and the Poisson ratio ν are usually determined by uniaxial loading of the body. In order to measure numerically the elastic properties of our simulated material we apply uniaxial loading on a two dimensional rectangular sample, which has linear extensions L in the direction of the loading and S in the perpendicular direction. The corresponding changes of the extensions due to loading are denoted by ΔL and ΔS. During the simulations plane-stress conditions are used, i.e. it is assumed that there is no stress in the direction out of the plane of the material. The boundaries parallel to the loading are free in the simulation.

In the case of uniaxial loading of a rectangular sample under plane - stress conditions, the Young modulus K is the ratio between the external force F per unit length acting on the solid and the strain in the direction of the loading, $F/S = \mathrm{K}\ \Delta L/L$. The Poisson ratio ν is the ratio between the strain in the direction perpendicular to the loading and the strain in the direction of the loading, $\Delta S/S = -\nu \Delta L/L$.

To avoid the disturbing effect of the elastic waves induced by the loading, the numerical experiment is performed in the following way (see also [14, 15]): The two opposite horizontal boundaries of the solid start to move with zero initial velocity and a constant, non-zero acceleration. When a certain velocity is reached the acceleration is set to zero and the velocity of the boundaries is kept fixed. With this slow loading the vibrations of the solid can be reduced drastically compared to the case when the boundaries start to move with non-zero initial velocity. A further way to suppress artificial vibrations is to introduce a small dissipation (friction or damping) between the grains. This dissipation has to be small enough not to affect the quasi-static results. To obtain the values of K and ν, the force acting on the boundary layer, and the horizontal and vertical extensions of the sample were monitored during the loading.

Figure 4 shows an example of the results of the measurement of the Young modulus, the horizontal stress $\sigma = F/S$ as a function of the vertical strain $\epsilon = \Delta L/L$. The values of K were extracted from

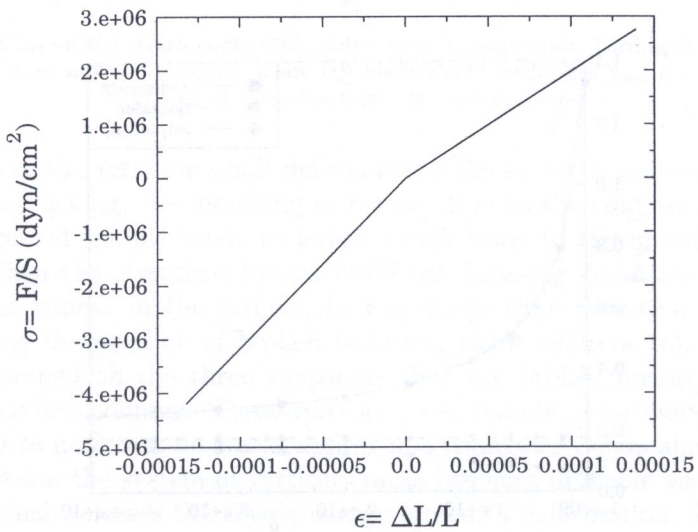

Fig. 4. Typical result of a measurement of the effective Young modulus K, the horizontal stress $\sigma = F/S$ as a function of the vertical strain $\epsilon = \Delta L/L$. Positive and negative strain means elongation and compression of the solid, respectively. The values of K were extracted from the slopes of the straight lines. One can observe the asymmetry of elongation and compression

the slope of the straight lines. It can be seen that elongation and compression of the system are not symmetric. The solid is more stiff under compression. The reason of the asymmetry is that in the case of elongation practically only the beams act but under compression one measures the common effect of the beams and the overlap force giving rise to a larger effective Young modulus.

Calculations were performed for elongation and compression of the sample fixing the value of the grain bulk Young modulus Y and varying the beam Young modulus E. The results for K are shown in Fig. 5. In the case of elongation K is a linear function of E as expected. For large E the elongation and compression curves are parallel. The difference between them is determined by the grain bulk Young modulus Y and by the geometry of the Voronoi tessellation. Small values of E compared to Y means that the cohesive force in the solid is small with respect to the repulsive overlap force. Under compression the polygons can move perpendicular to the loading in the direction of the free boundaries in the limiting case of small cohesion. Because of the dense packing (the initial packing fraction is one) the deformation tends to increase the overall volume resulting in dilatancy [2]. This

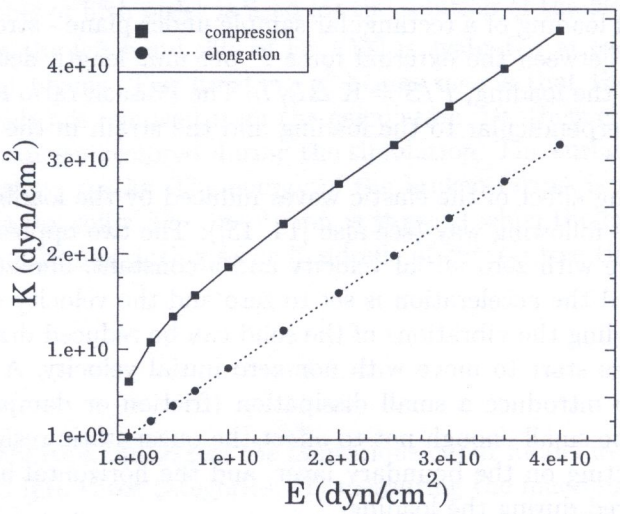

Fig. 5. The effective (macroscopic) Young modulus K of the granular solid measured under compression and elongation varying the beam Young modulus E between $10^9 \mathrm{dyn/cm}^2$ and $4 \cdot 10^{10} \mathrm{dyn/cm}^2$. The grain bulk Young modulus was fixed to be $Y = 10^{10} \mathrm{dyn/cm}^2$

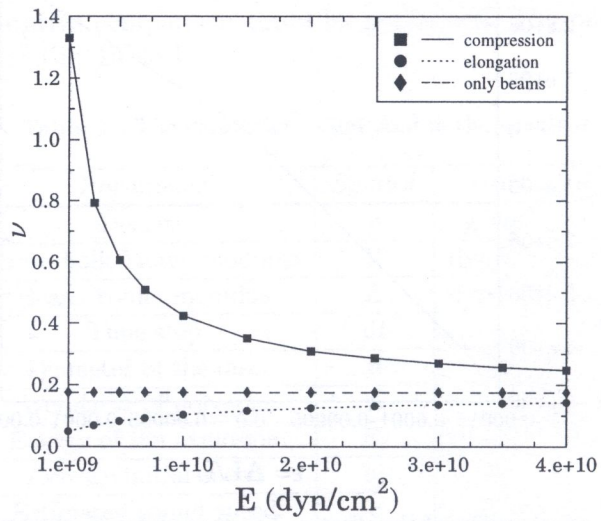

Fig. 6. The Poisson ratio of the granular solid measured under compression and elongation. The values of E and Y are the same as in Fig. 5. The curve of the pure beam lattice was obtained by switching off the overlap force between the polygons

effect gives rise to a small effective Young modulus, such that K is even smaller than the grain bulk Young modulus Y.

For the Poisson ratio ν a similar asymmetry of elongation and compression is observed as shown in Fig. 6. The values of ν for elongation are smaller than for compression but for large E both values approach the Poisson ratio of the pure beam lattice. In the limiting case of small cohesion ν can even exceed unity, due to the dilatancy mentioned above.

3.2. Compressive strength test

The simplest application of the model to study fracture of solids was the simulation of the compressive failure of a material. The simulations were performed on a rectangular sample of 25×40 elements with confined horizontal boundaries, as illustrated in Fig. 7. The strain controlled quasi-static loading was imposed similar to the measurement of the macroscopic elastic moduli. The confinement of the horizontal boundaries was ensured by fixing the horizontal coordinates and the rotation angle of the polygons in the horizontal boundary layers, while the vertical boundaries were allowed to move freely.

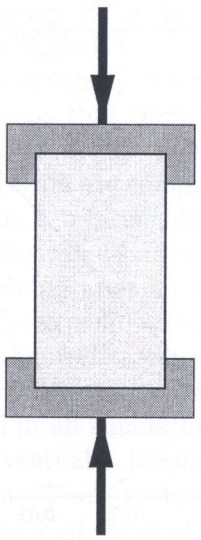

Fig. 7. The configuration of the strain controlled compressive strength test. During the simulations the two horizontal boundaries were moved vertically, while the horizontal coordinates and the rotation angle of the polygons of these boundary layers were fixed

In the early stages of the test, for small deformations the material behaves elastically. Further compression results in cracking, i.e. breaking of beams. Due to the confinement of the horizontal boundaries the compressed sample tends to bulge, which leads to the creation of tensile stresses on vertical planes. When the stretched beams fulfill the breaking condition Eq. (13) the beams break and microcracks appear in the sample. In Fig. 8 the time evolution of the crack pattern is presented by showing the position of broken beams at three different times during the loading process. It can be observed on the three snapshots that the broken beams form vertical cracks which divide the sample into columns. These vertical cracks mainly occur along the diagonals of the sample. It is important to note that no cracks appear in a triangular region along the confined walls. Under further compression the system of vertical cracks becomes unstable and the solid undergoes catastrophic failure, which releases the elastic energy stored in deformation. This breakage picture obtained by the simulations is consistent with the experimental observation.

Figure 9 shows the stress-strain relation for the compressive strength test. As it is expected for brittle materials the response of the solid is linear until it fails abruptly. The failure strain is identified with the position of the maximum of the $\sigma(\epsilon)$ curve.

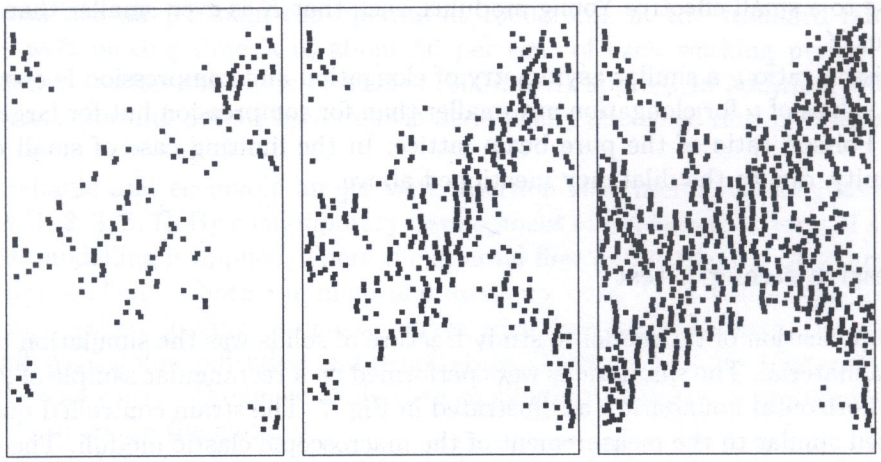

Fig. 8. The position of broken beams in the compression test. It can be observed that the cracks tend to form vertical columns parallel to the direction of the load, while two cones (i.e. two triangles in two dimensions) at the confined boundaries are practically intact

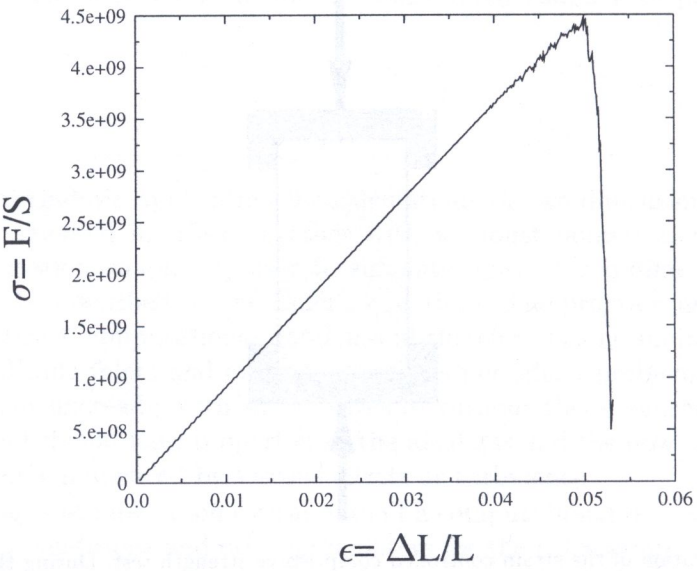

Fig. 9. The stress-strain relation during the compressive strength test

3.3. Fragmentation of solids

Recently, the fracture and fragmentation of granular solids has attracted considerable scientific and industrial interest. The length scales involved in this process range from the collisional evolution of asteroids to the degradation of materials comprising small agglomerates employed in industrial processes. On the intermediate scale there are several industrial and geophysical examples concerning the usage of explosives in mining and oil shale industry, fragments from weathering, coal heaps, rock fragments from chemical and nuclear explosions. Most of the measured fragment size distributions exhibit power law behavior with exponents between 1.9 and 2.6 concentrating around 2.4. Power law behavior of small fragment masses seems to be a common characteristic of brittle fracture [1, 5, 7, 11, 12, 13, 19]. Beside the size distribution of the debris, there is also particular interest in the energy required to achieve a certain size reduction. Collision experiments revealed that the mass of the largest fragment normalized by the total mass shows power law behavior as a function of the specific energy, i.e. imparted energy normalized by the total mass [1, 5, 11].

The catastrophic fragmentation of solids will be studied in two different experimental situations: through an explosion which takes place inside the solid and through the impact with a projectile (stroke with a hammer). We present a detailed analysis of the wave propagation, crack nucleation and crack growth, the time evolution of the fragmenting system, and of the size distribution of fragments. The application of our model to study the collision of macroscopic bodies was published in [8, 9].

3.3.1. Explosion of a disc shaped solid

In the explosion experiment the detonation takes place in the center of a solid disc. The granular solid with disc-like shape was obtained starting from the Voronoi tessellation of a square and cutting out a circular disc in the center, see Fig. 3.

In the center of the solid we choose one polygon, which plays the role of the explosive. Initial velocities are given to the neighboring polygons perpendicular to their common sides with the central one. The sum of the initial linear momenta has to be zero, reflecting the spherical symmetry of the explosion. From these two constraints it follows that for a polygon having mass m and a common boundary of length S with the explosive center, the initial velocity is proportional to S/m. The sum of the initial kinetic energies defines the energy E_o of the explosion. (For the parameter values and the initial conditions of the simulation see Table 1.)

As a result of these initial conditions a circularly symmetric outgoing compression wave is generated in the solid. In our context this means that there is a well-defined shell where the average longitudinal strain of the beams $\langle \epsilon \rangle = \langle \Delta l/l \rangle$ is negative. This compression wave is not homogeneous in the sense that not all the beams in this region are compressed. If the angle of a beam with respect to the radial direction is close to $\pi/2$ a beam can be slightly elongated within the compression wave.

Since the overall shape of the solid has the same symmetry as the compression wave it is possible to avoid geometrical asymmetries, which would arise for example in the explosion of a rectangular sample due to the corners. In the disordered solid the initial compression wave gives rise to a complicated stress distribution, in which the over-stressed beams break according to the breaking rule Eq. (13). The simulation is stopped if there is no beam breaking during 300 successive time steps. Free boundary conditions were used in all simulations.

Due to the beam breaking the solid eventually breaks apart, i.e. at the end of the process it consists of well separated groups of polygons. These groups of polygons, connected by the remaining beams, define the fragments. In the simulation of the explosion we are mainly interested in the time evolution of the fragmentation process and the mass distribution of fragments at the end of the process.

In the time evolution of the explosion two regimes can be distinguished. The initial regime is controlled by the compression wave and the disorder of the solid. The amplitude of the shock wave is proportional to the ratio of the average initial velocity of the polygons to the longitudinal sound speed of the solid. The width and the speed of the wave are mainly determined by the grain size and the Young moduli.

Since the beams are not allowed to break under compression the compression wave can go outward almost unperturbed and an elongation wave is formed behind it. Due to the elongation wave a highly damaged region is created in the vicinity of the explosive center where practically all the beams are broken and all the fragments are single grains. This highly damaged region is called the mirror spot. Since the breaking of the beams, i.e. the formation of cracks in the solid, dissipates energy after some time the growth of the damage stops. The size of this mirror spot is determined by the initial energy of the explosion, by the dissipation rate and by the breaking thresholds (see Fig. I).

During and after the formation of the mirror spot when the outgoing compression and elongation waves go through the solid, the weakest (i.e. the longest and thinnest) beams break in an uncorrelated fashion creating isolated cracks in the system. The uncorrelated beam breaking is dominated by the quenched disorder of the solid structure. This first uncorrelated regime of the explosion process lasts till the compression wave reaches the free boundary of the solid.

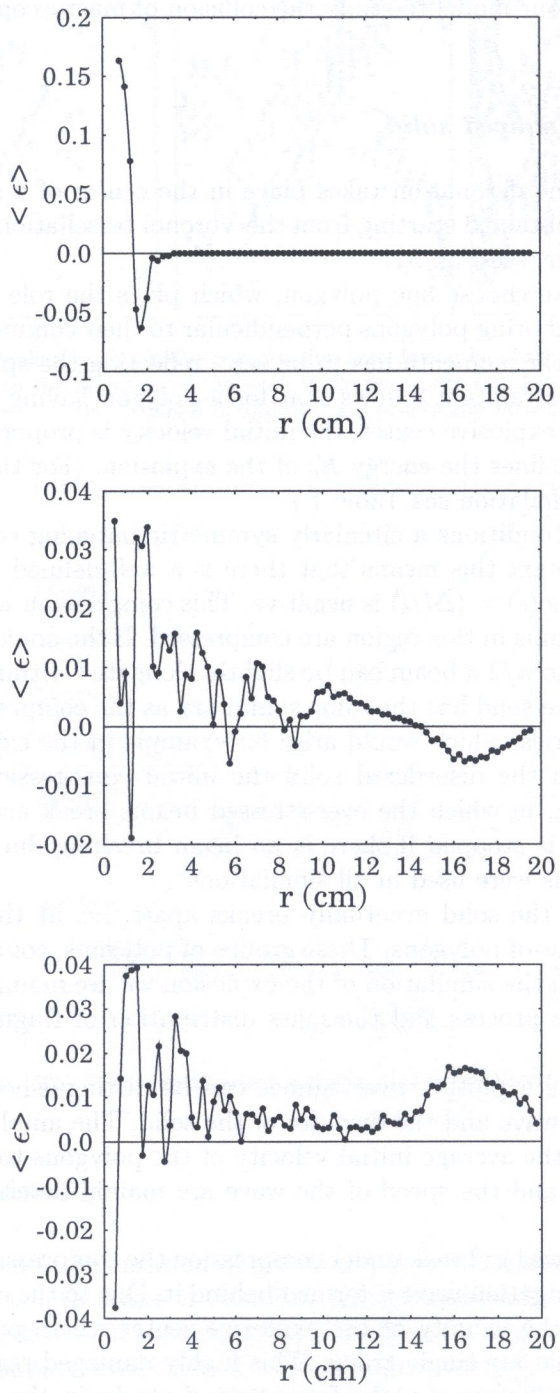

Fig. 10. Propagation of the elastic wave in the disc - shaped solid. (a) after $t = 10^{-5}$ s of the initial hit, (b) after $t = 3 \cdot 10^{-4}$ s the compression wave is approaching the boundary and (c) after $t = 5 \cdot 10^{-4}$ s the constructive interference of the incoming and the outgoing elongation waves

From the free boundary the compression wave is reflected back with opposite phase generating an incoming elongation wave. The constructive interference of the incoming and outgoing elongation waves gives rise to a highly stretched zone close to the boundary. The beams having small angle with respect to the radial direction have the largest elongation. In this zone a large number of beams break causing usually the complete break-off of a boundary layer along the surface of the solid. The thickness of this detached layer is roughly half the width of the incoming elongation wave (see Fig. I). The fragments of this boundary layer fly away in the radial direction with a high velocity carrying with them a large portion of the total energy in the form of their kinetic energy. After that the system starts to expand. This overall expansion initiates cracks going from inside to outside and from outside to inside. The branching of single cracks and the interaction of different cracks give rise to the final fragmentation of the solid (Fig. I). This second part of the evolution of the explosion process is dominated by the correlation of the cracks.

The propagation of the elastic waves, when the beam breaking is switched off, is presented in Fig. 10. One can observe the peak of the initially imposed shock, the propagation of the compression and elongation waves and the formation of the highly stretched zones at the boundary.

We performed simulations alternatively fixing the two breaking parameters t_ϵ and t_Θ and changing the value of the other one, keeping all the other parameters of the simulations fixed. In both cases the mass distribution of fragments was obtained. The fragment mass histograms are presented in Fig. 11. The lower cutoff of the histograms is determined by the size of the unbreakable polygons (smallest fragments), while the upper cutoff is given by the finite size of the system (largest fragment).

It can be observed that increasing the value of the varied parameter the distributions tend to a "limiting curve", but the histograms follow a power law for practically all the parameter pairs for at least one order of magnitude in mass:

$$F(m) \sim \alpha m^{-\beta}. \tag{15}$$

The effective exponents β were obtained from the estimated slopes of the curves. Apart from the case of extremely small breaking parameters the exponent β only slightly varies around $\beta = 2.0$, indicating a more or less universal behavior within the accuracy, with which β was determined (± 0.05). These values of the exponent β obtained numerically are in reasonable agreement with most of the experimental results.

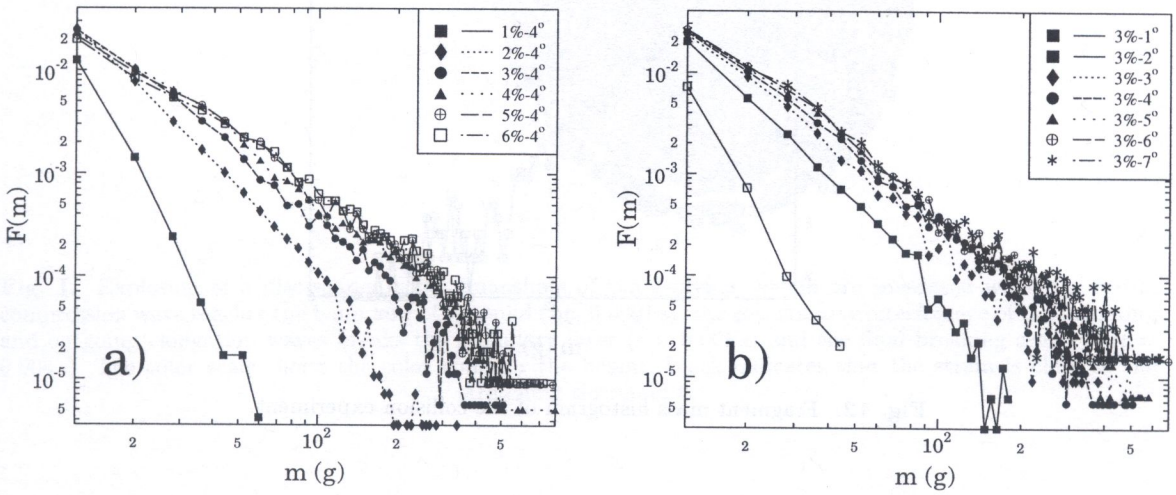

Fig. 11. (a) The fragment mass histograms varying the stretching threshold $t_\epsilon = 1\%-6\%$. The bending threshold is fixed $t_\Theta = 4°$. The contribution of the single polygons are ignored. For increasing t_ϵ the curves tend to a limit, which is determined by the fixed bending mode. (b) The fragment mass histograms varying the bending threshold $t_\Theta = 1°-7°$. The stretching threshold is fixed $t_\epsilon = 3\%$. For increasing t_Θ the curves tend to a limit, which is determined by the fixed stretching mode

3.3.2. Impact of a projectile with a solid block

Besides the explosion a catastrophic fragmentation of solids can also be generated by an impact with a projectile. In nature one of the most spectacular examples is that the size distribution of meteorites and asteroids shows power law behavior. These objects are believed to have originated from the fracture of primitive planets due to collisions [19, 5].

We applied our model to study the fragmentation of a rectangular solid block (e.g. a block of concrete) due to an impact. One polygon at the lower middle part of the block is given a high velocity directed inside the block simulating an elastic collision with a projectile. The boundary conditions and the stopping condition were the same as in the explosion experiment. The breaking thresholds were chosen $t_\epsilon = 3\%$ and $t_\Theta = 4°$.

The evolution of the fragmenting solid block is presented in Fig. II. As in the case of the explosion, the initially generated compression wave plays a significant role. Since the energy of the collision is concentrated around the impact site of the projectile the damage is the largest in that region. The completely destroyed zone, where all the beams are broken stretches inside the solid in the forward direction resulting in the break-up of the solid. When the shock wave reaches the boundary at the side of the solid opposite to the collision point it gives rise to the break-off of a boundary layer. The fragments of this layer fly away in the forward direction with a high velocity. Some small fragments from the vicinity of the collision point are scattered backward. The damage in the direction perpendicular to the projectile is not strong, the broken boundary layer is thicker and the speed of the fragments is smaller.

Results of laboratory experiments on high velocity impacts can be found in [19, 5, 1, 11, 12, 13]. In [11] a picture series obtained by a high speed camera is presented showing the time evolution of an impact experiment. Our results are qualitatively in good agreement with the experimental observations.

The resulting fragment mass histogram $F(m)$ is presented in Fig. 12. Similarly to the explosion experiment, $F(m)$ shows power law behavior for approximately one order of magnitude in mass. The value of the effective exponent is $\beta = 1.98 \pm 0.05$, which agrees well with most of the experimental results.

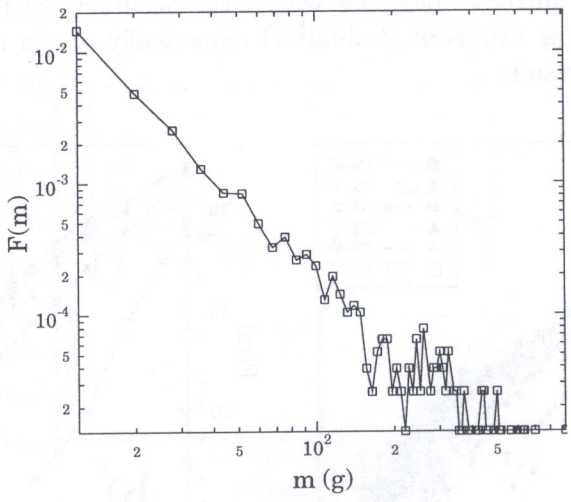

Fig. 12. Fragment mass histogram of the collision experiment.

4. Conclusions

We presented a two-dimensional discrete model of solids connecting unbreakable, undeformable elements by breakable, elastic beams. To demonstrate the capabilities of the model in the study of

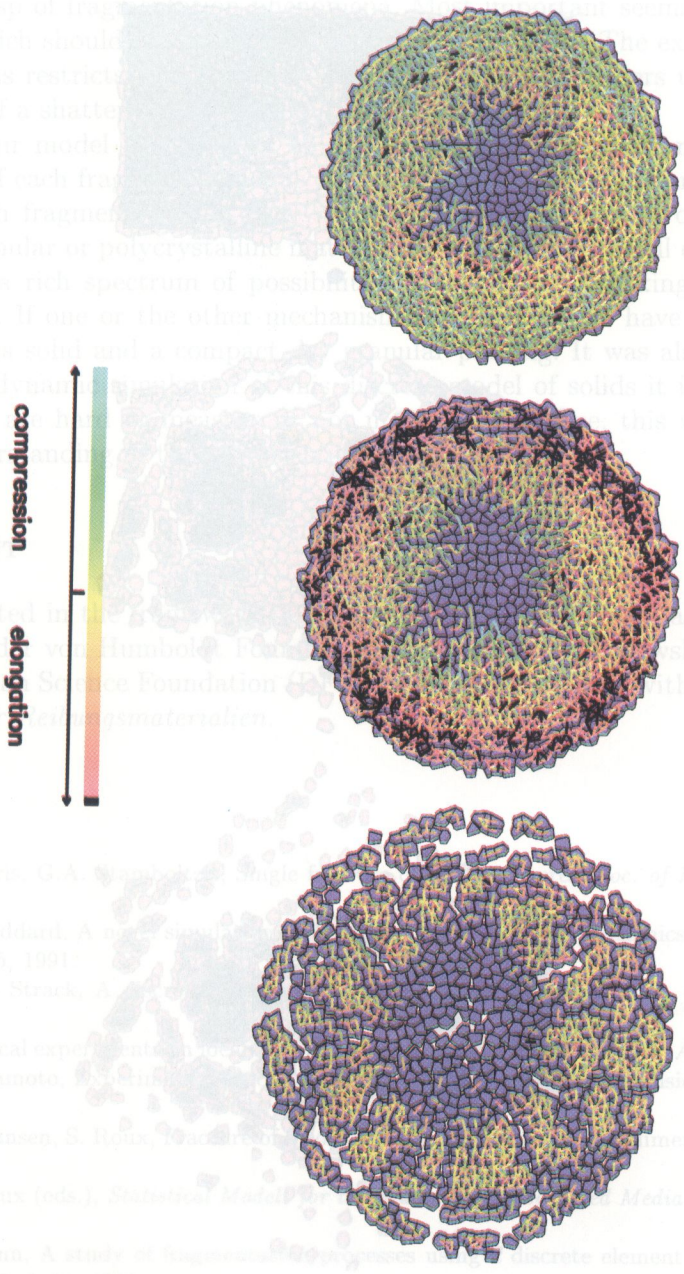

Fig. I. Explosion of a disc-shaped solid. Snapshots of the evolving system are presented when the initial compression wave reaches the boundary of the solid ($t = 0.0001$ s), the constructive interference of the incoming and outgoing elongation waves breaks the boundary layer ($t = 0.001$ s) and the final breaking scenario ($t = 0.004$ s). The color scale shows the color code for the beams. Black indicates that the strain is close to the stretching threshold t_ϵ

Fig. II. Fragmentation of a concrete block composed of elastic grains. One grain at the lower middle part of the block is given a high velocity directed inside the block. Here the velocity was 400 m/s. The size of the block was chosen to be 40cm × 20cm. Snapshots of the evolving system are presented at $t = 0.0004$ s, $t = 0.0015$ s and $t = 0.003$ s

fracture and fragmentation processes we performed simulations of a compressive strength test of a rectangular block and catastrophic fragmentation of solids due to impact and explosion. The results of the simulations were found to be in reasonable agreement with the experimental observations.

Still our study makes a certain number of technical simplifications which might be important for a full quantitative grasp of fragmentation phenomena. Most important seems to us the restriction to two dimensions, which should be overcome in future investigations. The existence of elementary, non-breakable polygons restricts fragmentation on lower scales and hinders us from observing the formation of powder of a shattering transition [7].

An advantage of our model with respect to most other fragmentation models is that we can follow the trajectory of each fragment, which is often of big practical importance and that we know how much energy each fragment carries away. The polygonal structure of our solid allows us to realistically model granular or polycrystalline matter, and considering as well cell repulsion as beam connectivity gives us a rich spectrum of possibilities ranging from breaking through bending to the effect of dilatancy. If one or the other mechanism is turned off we have the extreme cases of an elastic homogeneous solid and a compact dry granular packing. It was also demonstrated that during the molecular dynamic simulation of this discrete model of solids it is possible to monitor such quantities which are hard to measure or not measurable. Hence, this way of treatment can provide a deeper understanding of the process studied.

Acknowledgment

This work was supported in the framework of the project SFB381. F. Kun acknowledges financial support of the Alexander von Humboldt Foundation (Roman Herzog Fellowship). G.A. D'Addetta is grateful to the German Science Foundation (DFG) for financial support within the research group *Modellierung kohäsiver Reibungsmaterialien.*

References

[1] N. Arbiter, C.C. Harris, G.A. Stamboltzis, Single fracture of brittle spheres. *Soc. of Min. Eng.,* **244**: 119–133, 1969.

[2] Y.M. Bashir, J.D. Goddard, A novel simulation method for the quasi-static mechanics of granular assemblages. *J. Rheol.,* **35**: 849–885, 1991.

[3] P.A. Cundall, O.D.L. Strack, A discrete numerical model for granular assemblages. *Géotechnique,* **29**: 47–65, 1979.

[4] P.A. Cundall, Numerical experiments on localization in frictional materials. *Ingenieur-Archiv,* **59**: 148–159, 1989.

[5] A. Fujiwara, A. Tsukamoto, Experimental study on the velocity of fragments in collisional breakup. *Icarus,* **44**: 142–153, 1980.

[6] H.J. Herrmann, A. Hansen, S. Roux, Fracture of disordered elastic lattices in two dimensions. *Phys. Rev.,* **B 39**: 637–643, 1989.

[7] H.J. Herrmann, S. Roux (eds.), *Statistical Models for the Fracture of Disordered Media.* North Holland, Amsterdam, 1990.

[8] F. Kun, H.J. Herrmann, A study of fragmentation processes using a discrete element method. *Comput. Meth. Appl. Mech. Eng.,* **138**: 3–18, 1996.

[9] F. Kun, H.J. Herrmann, Fragmentation of colliding discs. *Int. Jour. Mod. Phys.,* **C 7**: 837–855, 1996.

[10] K.B. Lauritsen, H. Puhl, H.J. Tillemans, Performance of random lattice algorithms. *Int. J. of Mod. Phys.,* **C 5**: 909–922, 1994.

[11] T. Matsui, T. Waza, K. Kani, S. Suzuki, Laboratory simulation of planetezimal collisions. *J. of Geophys. Res.,* **87 B13**: 10968–10982, 1982.

[12] M. Matsushita, T. Ishii, *Fragmentation of Long Thin Glass Rods.* Department of Physics, Chuo University, 1992.

[13] L. Oddershede, P. Dimon, J. Bohr, Self-organized criticality in fragmenting. *Phys. Rev. Lett.,* **71**: 3107–3111, 1993.

[14] A.V. Potapov, M.A. Hopkins, C.S. Campbell, A two-dimensional dynamic simulation of solid fracture, Part I: Description of the model. *Int. J. of Mod. Phys.,* **C 6**: 371–398, 1995.

[15] A.V. Potapov, M.A. Hopkins, C.S. Campbell, A two-dimensional dynamic simulation of solid fracture, Part II: Examples. *Int. J. of Mod. Phys.,* **C 6**: 399–425, 1995.

[16] S. Roux, Continuum and discrete description of elasticity and other rheological behavior. In [7]: 87–113.
[17] C. Thorton, K.K. Yin, M.J. Adams, Numerical simulation of the impact fracture and fragmentation of agglomerates. *J. Phys. D. Appl. Phys.*, **29**: 424–435, 1996.
[18] H.J. Tillemans, H.J. Herrmann, Simulating deformations of granular solids under shear. *Physica*, **A 217**: 261–288, 1995.
[19] D.L. Turcotte, Fractals and fragmentation. *J. of Geophys. Res.*, **91 B2**: 1921–1926, 1986.